Deteriorating beam finite element for nonlinear analysis of concrete structures under corrosion

Fabio Biondini[a]* and Matteo Vergani[b]

[a]*Department of Civil and Environmental Engineering, Politecnico di Milano, Piazza Leonardo da Vinci, 32, Milan 20133, Italy;* [b]*R4M Engineering, Milan, Italy*

(*Received 15 November 2013; final version received 19 March 2014; accepted 24 June 2014; published online 23 September 2014*)

1. Introduction

The structural performance of concrete structures is time-dependent due to ageing and environmental damage (Ellingwood, 2005). Damaging factors include the effects of the diffusive attack from aggressive agents, such as chlorides, which may involve corrosion of steel reinforcement and deterioration of concrete (CEB, 1992). The direct and indirect costs associated with steel corrosion and related effects, in particular for concrete bridges and viaducts, are generally very high (ASCE, 2013; NCHRP, 2006). It is therefore of major importance to promote a life-cycle design of durable concrete structures and infrastructures (Frangopol, 2011; Frangopol & Ellingwood, 2010).

The experimental evidence shows that the main effect of corrosion is the reduction of the cross-sectional area of the reinforcing steel bars (Gonzalez, Andrade, Alonso, & Feliu, 1995; Zhang, Castel, & François, 2009). Corrosion can also significantly affect the ductility of steel bars and lead to brittle failure modes (Almusallam, 2001; Apostolopoulos & Papadakis, 2008). Moreover, the formation of corrosion products can involve deterioration of concrete due to propagation of splitting cracks (Vidal, Castel, & Francois, 2004; Zhang et al., 2009), delamination and spalling of the concrete cover (El Maaddawy & Soudki, 2007; Li, Zheng, Lawanwisut, & Melchers, 2007; Pantazopoulou & Papoulia 2001). In addition, the corrosion process may affect the steel–concrete bond strength (Bhargava, Gosh, Mori, & Ramanujam, 2007; Lundgren, 2007).

The local effects of reinforcement corrosion can be limited based on simplified design criteria related to threshold values for concrete cover, water–cement ratio, amount and type of cement, among others (*fib*, 2006). However, a life-cycle design of durable structures cannot be based only on indirect evaluations of the effects of damage, but it needs proper methodologies to take into account the global effects of local damage phenomena on the overall system performance under uncertainty. To this aim, a probabilistic approach to lifetime assessment of concrete structures in aggressive environment has been proposed in previous works (Biondini, Bontempi, Frangopol, & Malerba, 2004a, 2006). This approach relies on general procedures and methods for time-variant nonlinear and limit analysis of concrete structures under static and seismic loadings (Biondini, Camnasio, & Palermo, 2014; Biondini & Frangopol, 2008).

Nonlinear analysis of corroded concrete structures can be based on complex two- or three-dimensional finite element modelling (Sànchez, Huespe, Oliver, & Toro, 2010). This approach is useful to investigate local stress distribution problems or to analyse the behaviour of structural components and members. However, the involved computational cost and the amount of data to be managed make this approach impractical for the analysis of entire structural systems, such as buildings and

*Corresponding author. Email: fabio.biondini@polimi.it

bridges. A structural modelling based on beam finite elements represents an effective alternative to obtain sufficiently accurate results at an affordable computational cost.

The formulation of beam finite elements for nonlinear analysis of corroded concrete structures can refer to lumped plasticity models, where nonlinearity is described at the cross-sectional level within critical regions where plastic hinges are expected to occur (Akiyama, Frangopol, & Matsuzaki, 2011; Biondini et al., 2014), or distributed plasticity models, where nonlinearity is defined at the material level in terms of nonlinear constitutive laws of concrete and steel (Biondini et al., 2004a). Compared to lumped plasticity models, beam elements with distributed plasticity usually provide higher accuracy and allow a more detailed modelling of reinforcing steel corrosion and concrete deterioration.

In this paper, the formulation of a three-dimensional deteriorating reinforced concrete (RC) beam finite element for nonlinear analysis of concrete structures under corrosion is presented. The proposed formulation accounts for both mechanical nonlinearity, associated with the constitutive laws of the materials, and geometrical nonlinearity, due to the second-order effects (Biondini, 2004; Biondini, Bontempi, Frangopol, & Malerba, 2004b; Bontempi, Malerba, & Romano, 1995; Malerba, 1998). Damage modelling considers uniform and localised (pitting) corrosion and includes the reduction of cross-sectional area of corroded bars, the reduction of ductility of reinforcing steel and the deterioration of concrete strength due to splitting cracks and spalling of concrete cover (Biondini, 2011; Biondini & Vergani, 2012). In the structural model, these effects are described through damage indices and corrosion can selectively be applied to damaged structural members with a different level of penetration in each reinforcing bar.

The presented developments focus on the deterministic evaluation of the structural effects of prescribed damage patterns and corrosion penetration levels. However, it is worth noting that the proposed formulation can be extended to include the time factor in a lifetime scale by modelling the diffusive process of aggressive agents leading to corrosion initiation and damage propagation, as well as to account for the uncertainty in material and geometrical properties, in the physical models of the deterioration process and in the mechanical and environmental stressors. These extensions allow to incorporate the nonlinear analysis in a probabilistic framework for life-cycle assessment and design of concrete structures exposed to corrosion (Biondini et al., 2004a, 2006).

The beam finite element is validated with reference to the results of experimental tests carried out on RC beams subjected to corrosion of steel reinforcement, including accelerated corrosion (Rodriguez, Ortega, & Casal, 1997) and natural corrosion (Castel, François, & Arliguie, 2000; Vidal, Castel, & François, 2007). The application to a statically indeterminate RC beam under different corrosion scenarios and increasing levels of corrosion penetration demonstrates the need of a proper evaluation of the global effects of local damage on the overall system performance. Finally, the three-dimensional nonlinear structural analysis of a RC arch bridge under different damage scenarios and corrosion penetration levels is presented. The results highlight the effectiveness of the proposed approach and its application potentialities in the design and assessment of concrete structures exposed to corrosion.

2. Corrosion modelling

Damage modelling includes the reduction of cross-sectional area of corroded bars, the reduction of ductility of reinforcing steel and the deterioration of concrete strength due to splitting cracks, delamination and spalling of the concrete cover. Although corrosion does not affect significantly the yielding strength of reinforcing steel bars (Apostolopoulos & Papadakis, 2008), a moderate reduction of steel strength may be observed for corroded bars with irregular distribution of cross-section loss (Du, Clark, & Chan, 2005). This effect is not considered in the applications studied in this paper, even though it could be easily incorporated in the damage model. The deterioration of steel-concrete bond strength and the effects of the bond-slip of corroded steel bars are also not investigated.

2.1. *Reduction of the cross-section of reinforcing bars*

The most relevant effect of corrosion is the reduction of the cross-section of the reinforcing steel bars. By denoting p as the corrosion penetration depth, the following dimensionless corrosion penetration index $\delta \in [0;1]$ is introduced (Biondini & Vergani, 2012):

$$\delta = \frac{p}{D_0}, \tag{1}$$

where D_0 is the diameter of the steel bar. The area A_s of a corroded bar can be represented as a function of the corrosion penetration index as follows:

$$A_s(\delta) = [1 - \delta_s(\delta)]A_{s0}, \tag{2}$$

where $A_{s0} = \pi D_0^2/4$ is the area of the undamaged steel bar and $\delta_s = \delta_s(\delta)$ is a dimensionless damage function which provides a measure of cross-section reduction in the range [0;1]. The damage function $\delta_s = \delta_s(\delta)$ depends on the corrosion mechanism.

In carbonated concrete without relevant chloride content, corrosion tends to develop uniformly on the

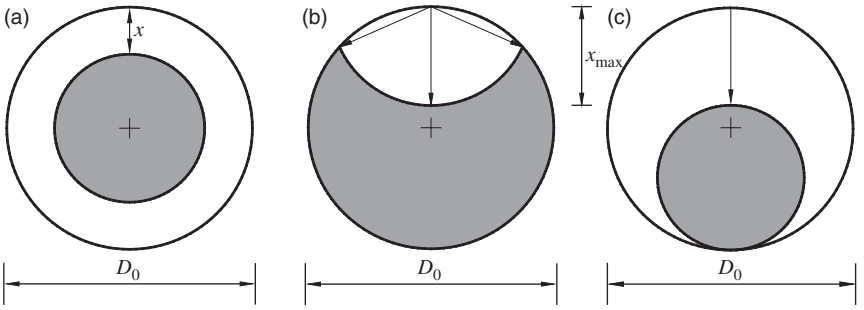

Figure 1. Modelling of cross-section reduction of a corroded reinforcing steel bar: (a) uniform corrosion; (b) pitting corrosion with circular pitting surface; and (c) pitting corrosion with a component of uniform corrosion.

reinforcing bars. Figure 1(a) shows a model of uniform corrosion where the reduction of the bar cross-section depends on the corrosion penetration depth $p = 2x$. This model is described by the following damage function:

$$\delta_s = \delta(2 - \delta). \tag{3}$$

In presence of chlorides, corrosion tends instead to localise (pitting corrosion). This type of corrosion can be characterised by means of a pitting factor R defined as the ratio between the maximum depth x_{max} measured at pit and the average penetration $\bar{x}$ calculated indirectly from the weight loss of the steel bar:

$$R = \frac{x_{max}}{\bar{x}}. \tag{4}$$

Typical values of the pitting factor vary between 4 and 8 for natural corrosion and between 5 and 13 for accelerated corrosion tests (Gonzalez et al., 1995). Regarding spatial distribution, there is no evidence that corrosion develops and propagates at concrete cracks. Instead, it tends to develop randomly where there are imperfections in the passive layer or interface defects (Zhang et al., 2009).

Pits have irregular shape and the cross-section reduction due to pitting corrosion is described through simplified models. As an example, the model shown in Figure 1(b) assumes a circular pitting surface with radius equal to the maximum penetration depth $p = x_{max}$ (Stewart, 2009; Val & Melchers, 1997). The model of pitting corrosion shown in Figure 1(c) is related to a mixed corrosion mechanism with a component of uniform corrosion (Rodriguez, Ortega, Casal, & Diez, 1996). With reference to the maximum penetration depth $p = x_{max}$, this model is described by the same damage function $\delta_s = \delta_s(\delta)$ of uniform corrosion and, with a pitting factor $R = 2$, leads to the same steel mass loss. This type of mixed corrosion mechanism can be found in accelerated corrosion tests, but it is not suitable to represent real cases where uniform or pitting corrosion are predominant (Zhang et al., 2009).

2.2. *Reduction of ductility of reinforcing bars*

Corrosion may significantly reduce the ductility of reinforcing steel bars. This is mainly related to the spatial variability of the attack penetration. Tensile tests on corroded bars show that for a quite limited mass loss (about 13%), reinforcing steel behaviour may become brittle (Almusallam, 2001). The results of experimental tests reported in Apostolopoulos and Papadakis (2008) indicate that ductility reduction is a function of the cross-section loss. Based on the fitting of available experimental results, the steel ultimate strain ε_{su} of a corroded bar is related to the damage index $\delta_s = \delta_s(\delta)$ as follows (Biondini & Vergani, 2012):

$$\varepsilon_{su} = \begin{cases} \varepsilon_{su0}, & 0 \le \delta_s < 0.016 \\ 0.1521\delta_s^{-0.4583}\varepsilon_{su0}, & 0.016 < \delta_s \le 1 \end{cases} \tag{5}$$

where ε_{su0} is the steel ultimate strain of the undamaged bar.

2.3. *Effects of corrosion on concrete*

The effects of corrosion are not limited to damage of reinforcing steel bars. In fact, particularly in case of uniform corrosion (Val, 2007), the formation of corrosion products may lead to the development of longitudinal cracks in the concrete surrounding the corroded bars and, consequently, to delamination and spalling of the concrete cover. This local deterioration of concrete can effectively be modelled by means of a degradation law of the effective resistant area of the concrete matrix A_c (Biondini et al., 2004a):

$$A_c = [1 - \delta_c(\delta)]A_{c0}, \tag{6}$$

where A_{c0} is the area of undamaged concrete and $\delta_c = \delta_c(\delta)$ is a dimensionless damage function which provides a measure of concrete damage in the range [0;1]. However, in this form, it may be not straightforward to establish a relationship between the damage function δ_c and the corrosion penetration index δ.

Alternatively, the effects of concrete deterioration can be taken into account by modelling the reduction of

concrete compression strength f_c due to longitudinal cracking (Biondini & Vergani, 2012):

$$f_c = [1 - \delta_c(\delta)]f_{c0}, \tag{7}$$

where f_{c0} is the strength of undamaged concrete. The reduced concrete strength f_c can be evaluated as follows (Coronelli & Gambarova, 2004):

$$f_c = \frac{f_{c0}}{1 + \kappa(\varepsilon_\perp/\varepsilon_{c0})}, \tag{8}$$

in which κ is a coefficient related to bar diameter and roughness ($\kappa = 0.1$ for medium-diameter ribbed bars), ε_{c0} is the strain at peak stress in compression and $\varepsilon_\perp$ is an average (smeared) value of the tensile strain in cracked concrete at right angles to the direction of the applied stress.

The transversal strain $\varepsilon_\perp$ is evaluated by means of the following relationship:

$$\varepsilon_\perp = \frac{b_f - b_i}{b_i} = \frac{\Delta b}{b_i}, \tag{9}$$

where b_i is the width of the undamaged concrete cross-section and b_f is the width after corrosion cracking. The increase of beam width Δb can be estimated as follows:

$$\Delta b = n_{bars} w, \tag{10}$$

where n_{bars} is the number of steel bars and w is the average crack opening for each bar. Several studies investigated the relationship between the amount of steel corrosion and the crack opening w (Alonso, Andrade, Rodriguez, & Diez, 1998; Zhang et al., 2009). The following empirical model is assumed (Vidal et al., 2004):

$$w = \kappa_w(\delta_s - \delta_{s0})A_{s0}, \tag{11}$$

in which $\kappa_w = 0.0575$ (mm^{-1}) and δ_{s0} is the amount of steel damage necessary for cracking initiation. This damage threshold is evaluated as follows:

$$\delta_{s0} = 1 - \left[1 - \frac{R}{D_0}\left(7.53 + 9.32\frac{c_0}{D_0}\right) \times 10^{-3}\right]^2, \tag{12}$$

where c_0 is the concrete cover.

The crack opening w increases with the expansion of corrosion products up to a critical width w_{cr} which corresponds to the occurrence of delamination and spalling of the concrete cover. Based on experimental evidence, delamination and spalling can occur for crack width in the range 0.1–1.0 mm (Al-Harthy, Stewart, & Mullard, 2011; Torres-Acosta & Martinez-Madrid, 2003; Vu, Stewart, & Mullard, 2005). In this study, a critical crack width $w_{cr} = 1$ mm is conventionally assumed.

The reduction of concrete strength is generally applied to the entire concrete cover (Coronelli & Gambarova, 2004). However, the longitudinal cracks pattern strongly depends on the arrangement of reinforcing bars. Cracking propagation induced by corrosion should be therefore limited to the zones adjacent to the corroded bars. With reference to a rectangular cross-section, Figure 2 shows a model where the reduction of concrete strength is applied only to a portion of concrete cover surrounding the corroded bars (Biondini & Vergani, 2012).

The cross-section is subdivided in cells and each concrete cell in the neighbourhood of a corroded bar is subjected to damage if at least one of its vertices lies in the intersection of the region surrounding the bar within a radius equal to the cover thickness and the region outside the centroidal circle passing through the bar. This model allows to effectively reproduce the mechanism of spalling of the concrete cover, characterised by inclined fracture planes for wide bar spacing (Figure 2(a)) and parallel fracture planes (i.e. delamination) for closely-spaced bars (Figure 2(b)).

3. Formulation of a deteriorating three-dimensional RC beam finite element

A three-dimensional RC beam finite element, capable to incorporate the effects of corrosion, is presented. The formulation assumes the linearity of the cross-sectional strain field and neglects shear failures and bond-slip of reinforcement. Mechanical nonlinearity, associated with the constitutive laws of the materials, and geometrical nonlinearity, due to the second-order effects, are taken into account (Biondini, 2004; Biondini et al., 2004b; Bontempi et al., 1995; Malerba, 1998).

The local reference system (x', y', z') of the beam finite element and the components of the vector of nodal

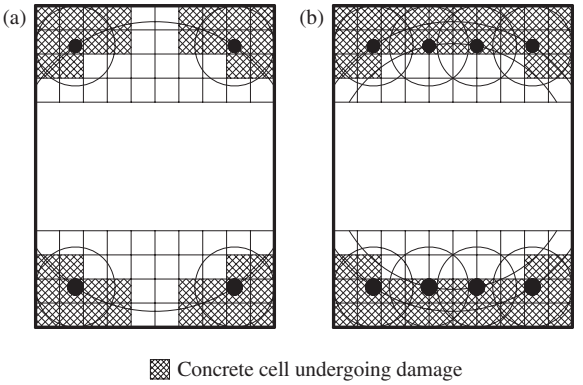

Figure 2. Definition of the zones of concrete cover undergoing damage: mechanism of cover spalling with (a) inclined fracture planes for wide bar spacing, and (b) parallel fracture planes (delamination) for closely spaced bars.

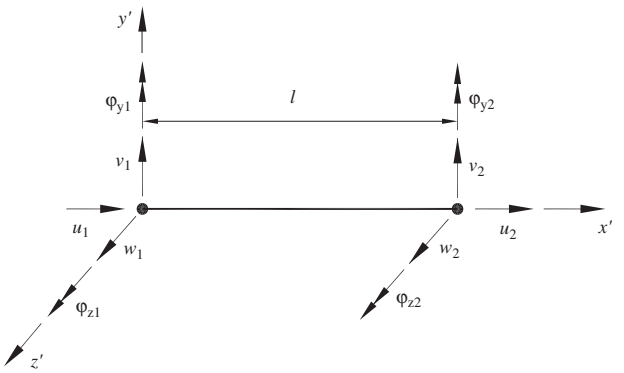

Figure 3. Local reference system and nodal displacements of the beam finite element.

displacements $\mathbf{s}' = [\mathbf{s}_a^{\mathrm{T}} | \mathbf{s}_b^{\mathrm{T}}]^{\mathrm{T}} = [u_1\ u_2 \,|\, v_1\ \varphi_{z1}\ v_2\ \varphi_{z2}\ w_1\ \varphi_{y1}\ w_2\ \varphi_{y2}]^{\mathrm{T}}$ are shown in Figure 3. The torsional degrees of freedom are not explicitly included in the formulation because torsion is assumed to be uncoupled from axial and bending deformations. The material $\mathbf{K}_{\mathrm{M}}$ and geometrical $\mathbf{K}_{\mathrm{G}}$ contributions to the element stiffness matrix $\mathbf{K}'$ and the vector of nodal forces $\mathbf{f}'$ equivalent to the applied loads $\mathbf{f}_0 = \mathbf{f}_0(x')$ are obtained by means of the principle of virtual work, in the form of the virtual displacements, and are evaluated by integration over the beam length l as follows:

$$\mathbf{K}' = \mathbf{K}_{\mathrm{M}} + \mathbf{K}_{\mathrm{G}}, \tag{13}$$

$$\mathbf{K}_{\mathrm{M}} = \int_0^l \mathbf{B}^{\mathrm{T}}\mathbf{H}\mathbf{B}\,\mathrm{d}x', \tag{14}$$

$$\mathbf{K}_{\mathrm{G}} = \int_0^l N\mathbf{G}^{\mathrm{T}}\mathbf{G}\,\mathrm{d}x', \tag{15}$$

$$\mathbf{f}' = \int_0^l \mathbf{N}^{\mathrm{T}}\mathbf{f}_0\,\mathrm{d}x', \tag{16}$$

where x' is the abscissa of the beam axis, $\mathbf{H} = \mathbf{H}(x')$ is the cross-sectional stiffness matrix, $N = N(x')$ is the axial force, $\mathbf{N} = \mathbf{N}(x')$ is the matrix of axial $\mathbf{N}_a = \mathbf{N}_a(x')$ and bending $\mathbf{N}_b = \mathbf{N}_b(x')$ displacement functions, $\mathbf{B} = \mathbf{B}(x')$ and $\mathbf{G} = \mathbf{G}(x')$ are the corresponding compatibility matrices:

$$\mathbf{N} = \begin{bmatrix} \mathbf{N}_a & \mathbf{0} \\ \mathbf{0} & \mathbf{N}_b \end{bmatrix}, \tag{17}$$

$$\mathbf{B} = \begin{bmatrix} \dfrac{\partial \mathbf{N}_a}{\partial x'} & \mathbf{0} \\ \mathbf{0} & \dfrac{\partial^2 \mathbf{N}_b}{\partial x'^2} \end{bmatrix}, \tag{18}$$

$$\mathbf{G} = \begin{bmatrix} \mathbf{0} & \dfrac{\partial \mathbf{N}_b}{\partial x'} \end{bmatrix}. \tag{19}$$

The matrix $\mathbf{N} = \mathbf{N}(x')$ is defined by adopting the Hermitian shape functions of a linear elastic beam having uniform cross-sectional stiffness and loaded only at its ends. However, due to material nonlinearity, the cross-sectional stiffness distribution along the beam is non-uniform even for prismatic members with uniform reinforcement. The stiffness matrix $\mathbf{H} = \mathbf{H}(x')$ is computed by integration over the area of the composite cross-section or by assembling the contributions of both concrete $\mathbf{H}_c = \mathbf{H}_c(x')$ and reinforcing steel $\mathbf{H}_{\mathrm{s}} = \mathbf{H}_{\mathrm{s}}(x')$:

$$\mathbf{H} = \mathbf{H}_c + \mathbf{H}_{\mathrm{s}}, \tag{20}$$

$$\mathbf{H}_c = \int_{A_c} \bar{E}_c \mathbf{b}^{\mathrm{T}}\mathbf{b}\,\mathrm{d}A, \tag{21}$$

$$\mathbf{H}_{\mathrm{s}} = \sum\nolimits_m \bar{E}_{\mathrm{sm}} \mathbf{b}_m^{\mathrm{T}}\mathbf{b}_m A_{\mathrm{sm}}, \tag{22}$$

where the symbol 'm' refers to the mth reinforcing bar located at point (y'_m, z'_m) in the centroidal principal reference system (y', z') of the cross-section, $\bar{E}_c = \bar{E}_c(x', y', z')$ and $\bar{E}_{\mathrm{sm}} = \bar{E}_{\mathrm{sm}}(x')$ are the secant moduli of the materials, and $\mathbf{b}(y', z') = [1\ \ -y'\ \ z']$ is the linear compatibility operator of the cross-sectional strain field. In this study, the stress-strain law of concrete is described by the Saenz's law in compression and a bilinear softening model in tension. For steel, a bilinear elastic-plastic model in both tension and compression is assumed.

The damage effects associated with the corrosion penetration index δ are included in this formulation by assuming $A_{\mathrm{s}} = A_{\mathrm{s}}(\delta)$ and $\varepsilon_{\mathrm{su}} = \varepsilon_{\mathrm{su}}(\delta)$ for the steel bars and $f_c = f_c(\delta)$ for the concrete to obtain the deteriorating stiffness matrices $\mathbf{H} = \mathbf{H}(x', \delta)$ and $\mathbf{K}' = \mathbf{K}'(\delta)$ (Biondini, 2011; Biondini & Vergani, 2012). It is worth noting that corrosion can selectively be applied to damaged structural elements with a different level of corrosion penetration for each reinforcing bar.

The quantities which define the characteristics of the beam finite element are evaluated by numerical integration. The volume of the element is subdivided in prismatic isoparametric sub-domains having quadrilateral cross-section, and each sub-domain is replaced by a grid of points whose location depends on the adopted integration rule (Bontempi et al., 1995). In particular, depending on the function to be integrated and the geometry of the problem, the Gauss-Legendre and the Gauss-Lobatto schemes are used.

Finally, by assembling the stiffness matrix $\mathbf{K}'$ and the vectors of nodal forces $\mathbf{f}'$ for all members in a global reference system (x, y, z), the equilibrium of the structure can be expressed as follows:

$$\mathbf{Ks} = \mathbf{f}, \tag{23}$$

where $\mathbf{K} = \mathbf{K}(\mathbf{s},\delta)$ is the overall stiffness matrix, $\mathbf{s} = \mathbf{s}(\delta)$ is the vector of nodal displacements and $\mathbf{f}$ is the vector of applied nodal forces. This nonlinear equation system is solved numerically by means of the secant method for prescribed values of the corrosion penetration index δ.

4. Validation of the RC beam finite element

The RC beam finite element is validated with reference to experimental tests carried out on beams with corroded reinforcement.

4.1. *Beams subjected to accelerated corrosion tests*

The experimental tests reported by Rodriguez et al. (1997) are considered. The validation procedure refers to the two type of beams shown in Figure 4. The beams were cast adding calcium chloride to the mixing water, subjected to an accelerated corrosion process with a current density of 100 μA/cm^2 and finally loaded up to failure.

The beams type 11, with a lower reinforcement ratio, showed a flexural failure with rupture of the tensile bars. For beams type 31, with a higher reinforcement ratio, a crushing failure of concrete in compression occurred. For these beams, the average corrosion penetration depth $\bar{x}$, as calculated indirectly from weight loss of the steel bars, and the maximum penetration depth x_{max} measured at pits are listed in Table 1. The mechanical properties of concrete and steel are listed in Tables 2(a) and 3(a), respectively.

The structural symmetry of the model is exploited and the half beam is discretised into six finite elements with five Gauss-Lobatto sampling points in each element. The cross-section is subdivided into 300 isoparametric sub-domains, with a grid of 3 × 3 Gauss-Lobatto sampling points in each domain. The cross-sectional area of the corroded bars is computed by assuming the model of pitting corrosion shown in Figure 1(c) with maximum penetration depth x_{max} for the bars in tension, and uniform corrosion with penetration depth $x = \bar{x}$ for the bars in compression (Table 1).

Table 1. Beams under accelerated corrosion: average corrosion penetration depth, as calculated indirectly from weight loss of the corroded steel bars, and maximum penetration depth measured at pits (value in parenthesis). Adapted from Rodriguez et al. (1997).

	Corrosion penetration depth (mm)	
Beam type	Tensile bars	Compressive bars
114	0.45 (1.1)	0.52
115	0.36 (1.0)	0.26
116	0.71 (2.1)	0.48
313	0.30 (1.3)	0.20
314	0.48 (1.5)	0.26
316	0.42 (1.8)	0.37

A comparison between the results of the nonlinear analyses and the results of the tests is shown in Figure 5 in terms of load versus midspan displacement diagrams. The good agreement between experimental and numerical results demonstrates the accuracy of the proposed formulation, as well as its capability to capture the main corrosion degradation mechanisms. With this regard, Figure 6 shows the cross-sectional contour maps of concrete damage of the beams 116 and 314. These maps highlight the important role of the reinforcement layout for the propagation of damage in the concrete cover. In fact, for the beams type 11, the corrosion of the steel bars located at the cross-section corners leads to a localised spalling along inclined fracture planes (Figure 6(a)). For the beams type 31,

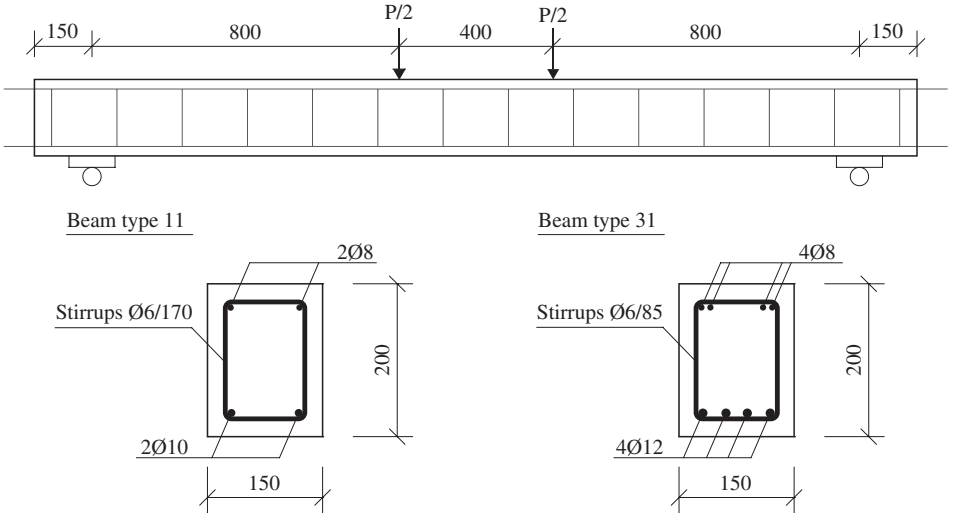

Figure 4. Experimental tests on beams subjected to accelerated corrosion: geometrical dimensions (mm), testing scheme and characteristics of the cross-sections for beams type 11 and type 31. Adapted from Rodriguez et al. (1997).

Table 2. Mechanical properties of concrete: (a) beams under accelerated corrosion, (b) beams under natural corrosion, (c) statically indeterminate beam, (d) arch bridge.

	Case study	Element type	f_c (MPa)	f_{ct} (MPa)	E_{c0} (GPa)
(a)	Beams under accelerated corrosion tests	Beam 111	50.0	4.1	37.3
		Beams 114-115-116	34.0	3.1	33.8
		Beam 311	49.0	4.1	37.1
		Beams 313-314-316	37.0	3.2	34.5
(b)	Beams under natural corrosion tests	Beam B1T	65.3	0.0	36.3
		Beam B1CL	63.4	0.0	35.0
(c)	Statically indeterminate beam	Beam	35.0	3.2	34.0
(d)	Arch bridge	Arches & Deck	35.0	3.2	34.0

Table 3. Mechanical properties of steel: (a) beams under accelerated corrosion, (b) beams under natural corrosion, (c) statically indeterminate beam, (d) arch bridge.

	Case study	Element type	f_{sy} (MPa)	f_{su} (MPa)	E_s (GPa)	ε_{su}
(a)	Beams under accelerated corrosion tests	Bars ø8	615	673	210	0.03
		Bars ø10	575	655	210	0.03
		Bars ø12	585	673	210	0.03
(b)	Beams under natural corrosion tests	Bars (B1T & B1CL)	500	500	210	0.06
(c)	Statically indeterminate beam	Bars	440	440	210	0.01
(d)	Arch bridge	Bars	440	440	210	0.01
		IPN I-beams	275	275	210	0.10
		Ties	1600	1600	200	0.10

a similar pattern of localised damage would occur at the top side of the cross-section for the steel bars arranged in pairs at the corners. The corrosion of the four closely-spaced steel bars at the bottom side leads instead to the delamination and spalling of the entire concrete cover (Figure 6(b)).

However, it is worth noting that the lower values of penetration depth of the bars in compression may be not sufficient to induce the spalling of concrete cover. This is illustrated in Figure 7, which shows the comparison between experimental and numerical results obtained with and without the activation of the spalling of the concrete cover at the top side of the cross-section for the beam 314. If cover spalling is activated, the numerical model underestimates the stiffness associated with the initial branch of the load–displacement diagram. As shown in Figure 7, these results are also in good agreement with the numerical results obtained by Sànchez et al. (2010). On the contrary, if cover spalling is not activated, the numerical results of the finite element analysis reproduce the initial branch of the load-displacement diagram with good accuracy.

4.2. Beams subjected to natural corrosion tests

The experimental tests reported by Castel et al. (2000) and Vidal et al. (2007), concerning beams subjected to natural corrosion, are considered. The tested beams were exposed to a salt fog (35 g/l of NaCl, corresponding to the salt concentration of sea water) and subjected to a three-point flexure up to collapse on a clear span of 2.8 m. The beams have rectangular cross-section 150 mm × 280 mm. They are reinforced with two bars with diameter $\phi = 12$ mm at the bottom side in tension and two bars with diameter $\phi = 6$ mm at the top side in compression, with a concrete cover $c_0 = 10$ mm. Based on the available information, the mechanical properties listed in Tables 2(b) and 3(b) for concrete and steel, respectively, are assumed. From the set of tested specimens, a non corroded control beam (B1T) and a beam after 14 years of exposure (B1CL) are considered for the validation procedure.

In the structural model the beam is discretised into six finite elements with five Gauss-Lobatto sampling points in each element. The cross-section is subdivided into 200 isoparametric sub-domains, with a grid of 3 × 3 Gauss-Lobatto sampling points in each domain. The nonlinear analysis of the corroded beam is performed by assuming a steel cross-section loss of 22%, which corresponds to the average value of the maximum cross-section losses measured for the two tensile reinforcing steel bars in the critical region at midspan (Castel et al., 2000). Figure 8 shows the comparison between experimental and numerical results in terms of load versus midspan displacement. The comparison confirms that the proposed formulation is able to reproduce with good accuracy the structural response of noncorroded and corroded structures and to provide a very accurate estimation of both the load carrying capacity and the maximum displacement at failure.

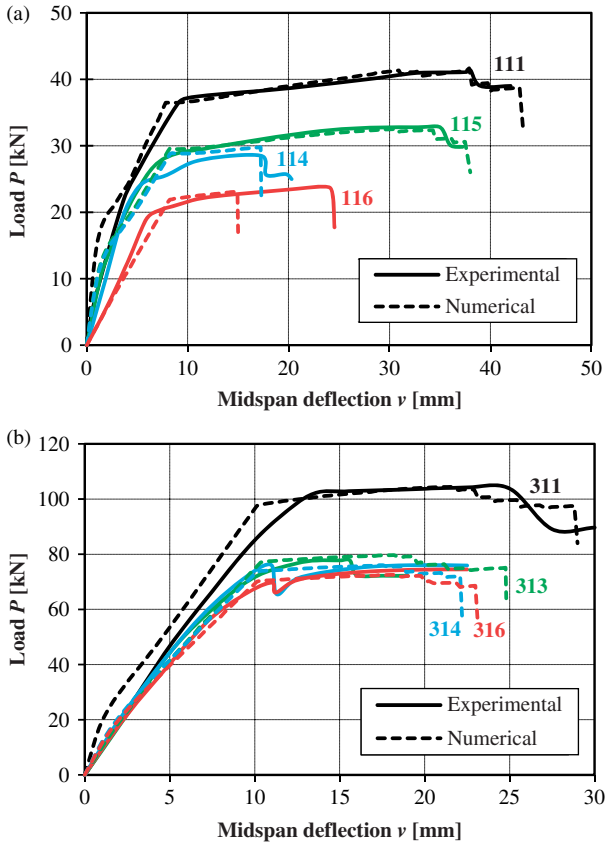

Figure 5. Beams under accelerated corrosion: comparison between experimental and numerical results for (a) beams type 11 and (b) beams type 31.

5. Applications

5.1. *Statically indeterminate beam*

The RC beam shown in Figure 9 is considered. The material properties of concrete and steel are listed in Tables 2(c) and 3(c), respectively. The structural response of the beam is investigated by assuming uniform corrosion of the longitudinal steel reinforcement localised over a length of 50 cm from the clamped end. Figure 10(a),(b) shows the deformed shape and the bending moment diagram,

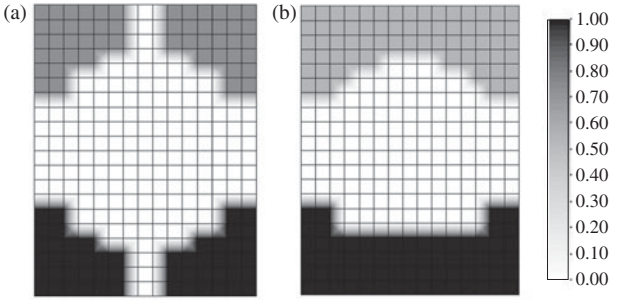

Figure 6. Beams under accelerated corrosion: cross-sectional contour maps of concrete damage of (a) beam 116 and (b) beam 314.

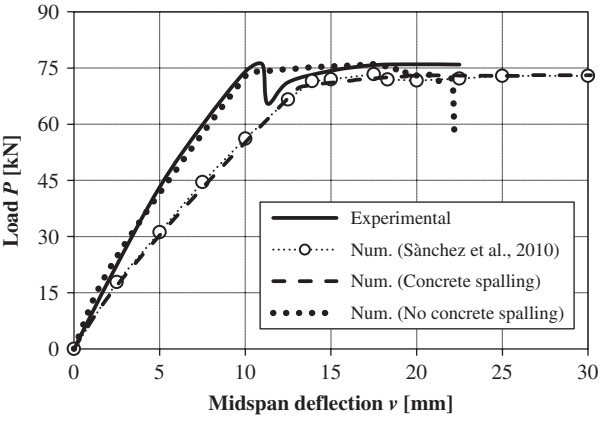

Figure 7. Beams under accelerated corrosion: comparison between experimental and numerical results, obtained with and without the activation of the spalling of the concrete cover, for the beam 314.

respectively, for increasing values of the corrosion penetration index δ. These results highlight the effects of localised damage on the global structural response. In the case studied, localised damage involves both an increase of the overall deformability of the beam and, due to statical indeterminacy, a redistribution of the internal stresses. In particular, the structural response of the damaged beam tends to reproduce the behaviour of a simply supported beam (dashed curve in Figure 10(a),(b)) when the corrosion penetration index approaches the limit value $\delta = 1$. This indicates that for statically indeterminate structures, the internal stresses under constant loading may change over time as a consequence of the time evolution of damage.

The role of the damage exposure scenario is also investigated by considering three cases of uniform corrosion distributed over the beam length, with corrosion of (I) top reinforcement only, (II) bottom reinforcement only and (III) both top and bottom reinforcement. Figure 11(a),(b) shows, for each case studied, the maximum beam deflection and the bending moment at the clamped beam end, respectively, versus the corrosion penetration index. It is worth noting that a sudden change of slope of these curves is related to damage thresholds leading to the first yielding of steel reinforcement. Figure 11(a) shows that corrosion leads to an increase of the beam deformability. As expected, the maximum increase of beam deflection is achieved for case (III), with corrosion of both top and bottom reinforcement. Moreover, the comparison of case (I) and case (II) highlights that corrosion of bottom reinforcement leads to higher values of beam deflection with respect to corrosion of top reinforcement. In terms of stress redistribution, the bending moment at the clamped beam end decreases for case (I), with corrosion of top reinforcement, and increases for case (II), with corrosion of bottom reinforcement, as the corrosion penetration index increases. For case (III), with corrosion of top and bottom reinforcement, the bending moment at the clamped beam

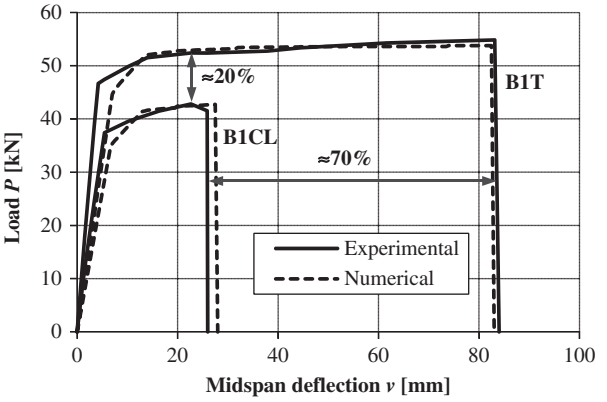

Figure 8. Beams under natural corrosion: comparison between experimental and numerical results.

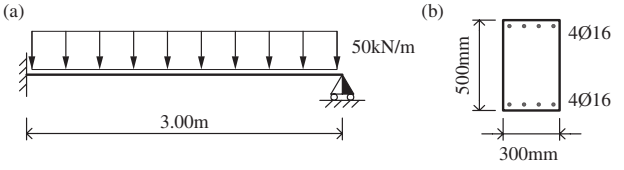

Figure 9. RC beam exposed to corrosion: (a) structural scheme and loading and (b) geometry of the cross-section and reinforcement layout.

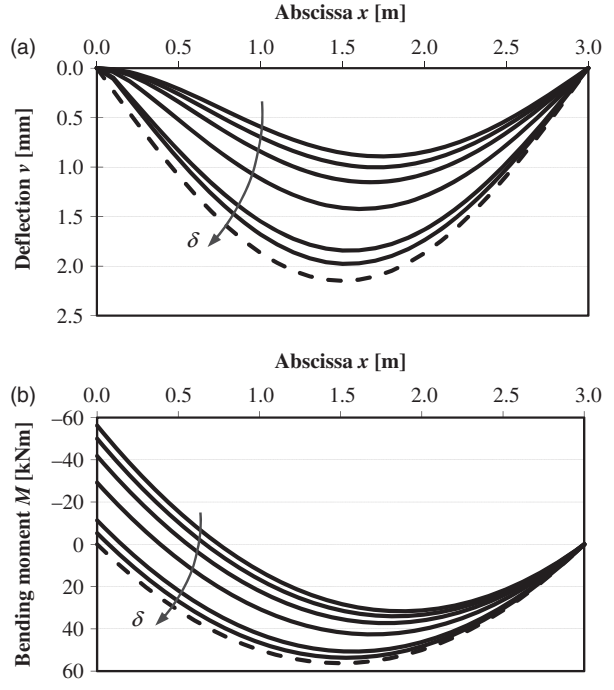

Figure 10. Statically indeterminate beam: (a) deformed shape and (b) bending moment diagram for different values of corrosion penetration depth ($\delta = 0$, 0.2, 0.4, 0.6, 0.8, 1.0), compared with the limit case of undamaged simply supported beam (dashed curve).

end does not change for corrosion levels up to the threshold value $\delta = 0.42$ associated with the first yielding of top reinforcement and decreases for increasing levels of corrosion $\delta > 0.42$ up to collapse.

Based on the results of this application, it is clear that design for durability of concrete structures cannot be limited to simplified prescriptions associated with the quality of the materials and structural details such as the minimum concrete cover, but also needs to rely on nonlinear structural analysis frameworks capable to take into account the global effects of local damage phenomena on the overall system performance.

5.2. Arch bridge

The structural response of a Nielsen type RC arch bridge with the deck suspended by inclined steel ties is investigated under different damage scenarios and corrosion penetration levels. Many structures of the same type were built in Europe in the Thirties, with spans varying between 50 and 140 m. Figure 12 shows the structural scheme and the main dimensions of the arch bridge, as well as the

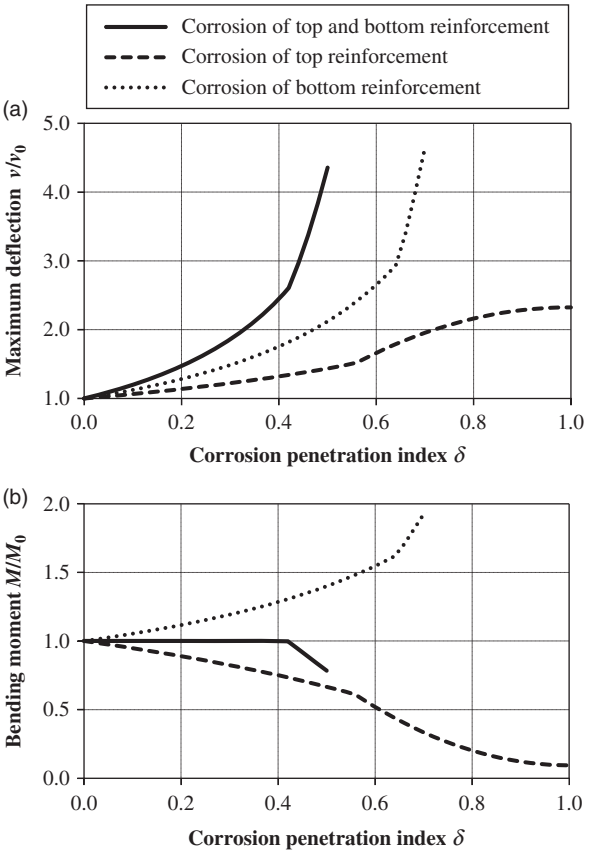

Figure 11. Statically indeterminate beam: damaged/undamaged ratio of (a) maximum deflection and (b) bending moment at the clamped end of the corroded beam versus the corrosion penetration index.

geometry, dimensions and reinforcement layout of the structural members. The three-dimensional structural model of the bridge is shown in Figure 13.

The span of the arch bridge is 90 m, subdivided into 12 sub-spans by the anchoring points of the suspension ties. The rise of the arches is 13 m. The static scheme allows the elimination of the horizontal thrust that is carried by means of two IPN 600 European standard steel I-beams inserted into the concrete main beams of the deck. The bridge deck is stiffened by transversal ribs with rectangular cross-section 250 mm × 640 mm and 3.75 m spacing. The arches are connected by seven transversal T-beams with top flange 700 mm × 200 mm and beam web 200 mm × 400 mm. The beams are located in correspondence with the anchoring points of some ties and at midspan, as shown in Figure 13. Further details about the geometry and reinforcement layout of the transversal beams of both deck and arches can be found in Vergani (2010). The suspension ties are steel bars with diameter $\phi = 70$ mm. The material properties of concrete and different types of steel are listed in Tables 2(d) and 3(d), respectively.

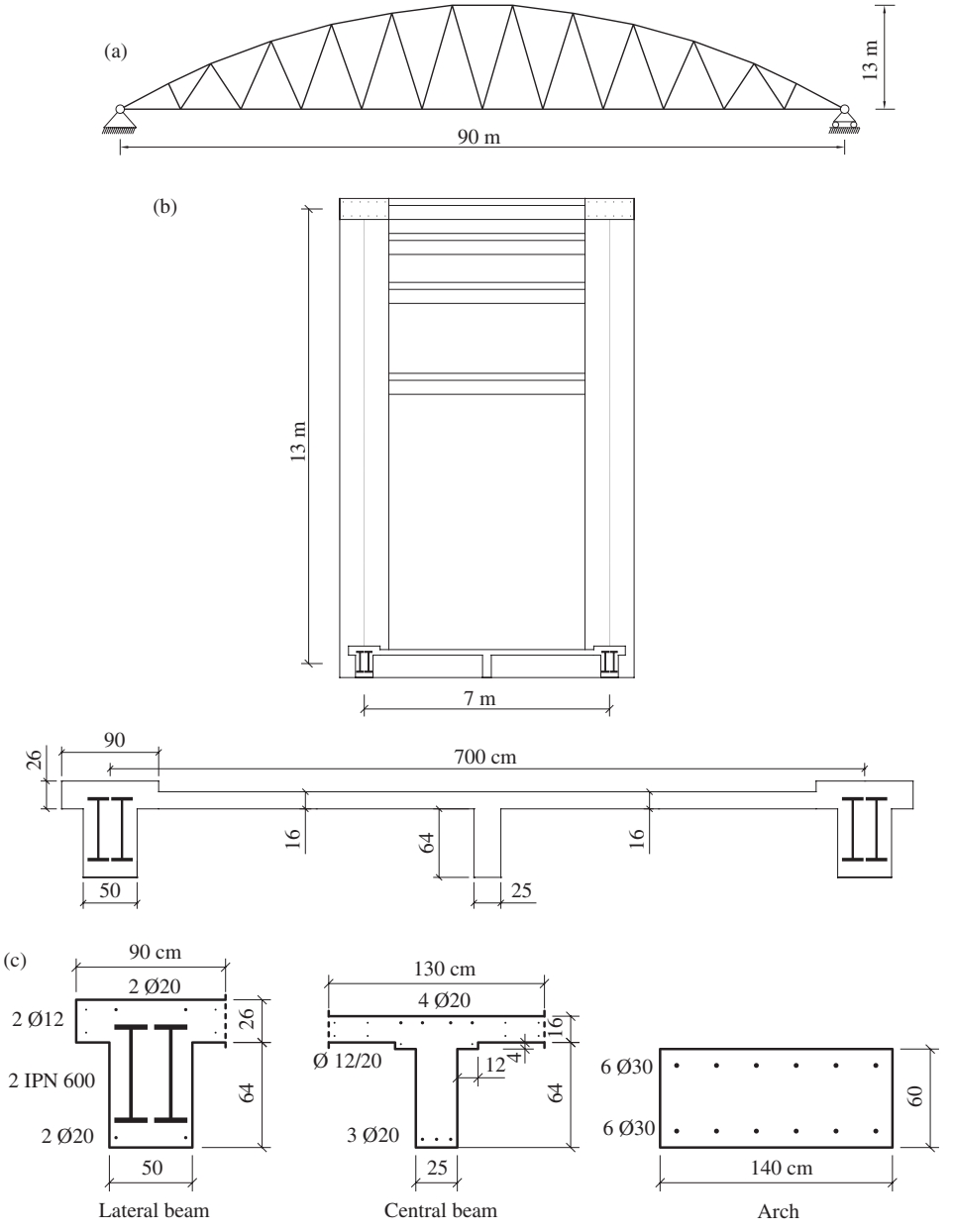

Figure 12. RC arch bridge exposed to corrosion: (a) structural scheme, (b) cross-section view of bridge deck and arches, and (c) cross-sections of the deck's main beams and of the arches.

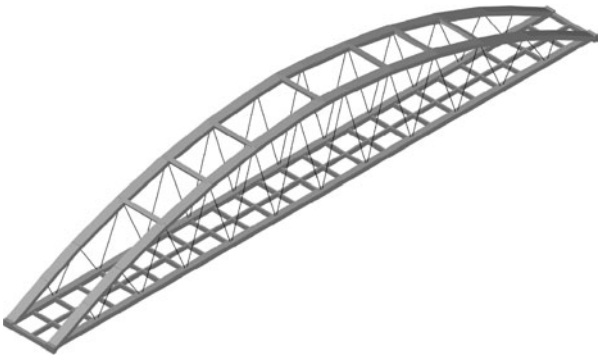

Figure 13. View of the three-dimensional structural model of the arch bridge.

The bridge deck is modelled by means of a grillage formed by the three longitudinal main beams and 25 transversal beams. The structural response of the bridge is analysed under the self weight $g_1 = 8\,\text{kN/m}^2$ and $g_2 = 21\,\text{kN/m}$ of the deck and the arches, respectively, and a live load q uniformly distributed over the deck area and increased up to collapse. The load associated with each grid unit $3.50\,\text{m} \times 3.75\,\text{m}$ of the deck grillage is applied to the corresponding edge beam elements.

The effects of corrosion on the bridge structural performance are investigated at the system level by considering three damage scenarios with corrosion applied separately to deck, arches and ties. The results of this type of analyses allow to clarify which are the structural elements that more significantly affect the structural performance if exposed to corrosion. This information could provide the basis to establish a hierarchy of protection techniques, as well as to plan proper maintenance actions and repair interventions.

The structural analyses are carried out by assuming uniform corrosion for prescribed values of corrosion

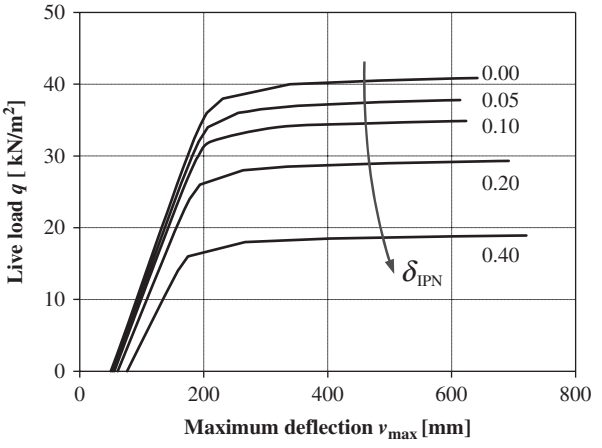

Figure 14. Arch bridge: load versus maximum deflection of the lateral main beams for different damage levels of the bridge deck ($\delta = \delta_{\text{IPN}} = 0,\ 0.05,\ 0.10,\ 0.20,\ 0.40$).

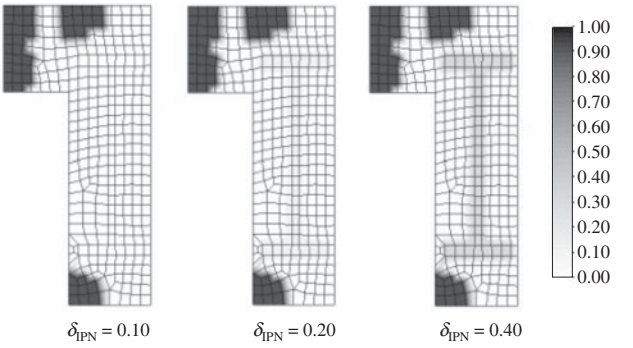

Figure 15. Arch bridge: contour maps of concrete damage of the lateral beams of the deck (half cross-section).

penetration depth for reinforcing steel bars, IPN I-beams and steel ties. For steel bars and steel ties, the damage level is described by using the corrosion penetration index δ. For the IPN I-beams, the level of corrosion is more conveniently described in terms of cross-section loss as follows:

$$\delta_{\text{IPN}} = 1 - \frac{A_{\text{IPN}}}{A_{\text{IPN},0}}, \tag{24}$$

where A_{IPN} is the area of the corroded steel beam, and $A_{\text{IPN},0}$ is the corresponding value in the undamaged state. Figure 14 depicts the load versus the maximum deflection of the lateral main beams for different damage levels of the bridge deck ($\delta = \delta_{\text{IPN}} = 0,\ 0.05,\ 0.10,\ 0.20,\ 0.40$). The results indicate that this damage scenario involves an increase of deformability and a significant decrease of load carrying capacity, with small changes in terms of displacement ductility. It is interesting to note that even for a limited damage of the IPN I-beams, the corrosion of the reinforcing steel bars may lead to the

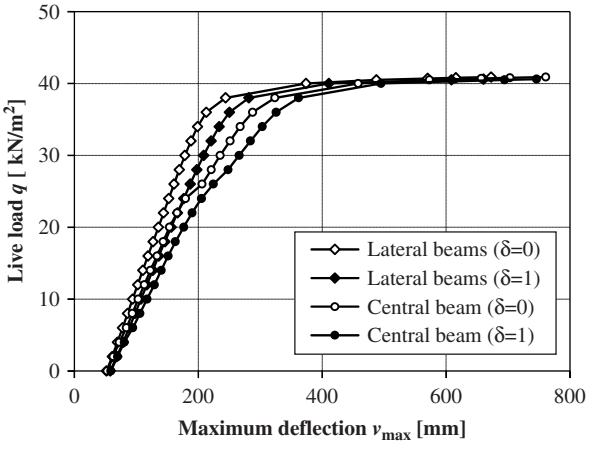

Figure 16. Arch bridge: load versus maximum deflection of the lateral and central main beams of the deck for the cases of undamaged bridge ($\delta = 0$) and bridge with damaged arches with complete corrosion penetration ($\delta = 1$).

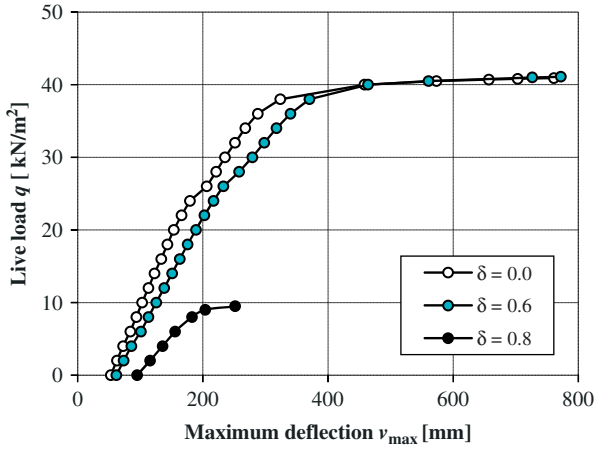

Figure 17. Arch bridge: load versus maximum deflection of the central main beam of the deck for the cases of undamaged bridge ($\delta = 0$) and bridge with damaged suspension steel ties with corrosion penetration depth $\delta = 0.6$ and $\delta = 0.8$.

spalling of the concrete cover, as shown by the cross-sectional damage contour maps in Figure 15.

The effects of corrosion applied to the arches are presented in Figure 16 in terms of load versus maximum deflection of the lateral and central beams of the deck for the cases of undamaged bridge ($\delta = 0$) and bridge with damaged arches with complete corrosion penetration ($\delta = 1$). The results show that the deterioration of the arches, which also involves the spalling of the concrete cover, does not significantly affect the structural performance.

Similar results are obtained when corrosion damage is applied to the suspension steel ties with a corrosion penetration depth up to $\delta = 0.60$, as shown in Figure 17. However, further cross-section reductions of the steel ties involve a remarkable deterioration of both load carrying capacity and ductility of the bridge structure, as shown in Figure 17 for $\delta = 0.80$, and lead to structural collapse under dead load for a corrosion penetration depth $\delta = 0.87$. Figure 18 shows the effect of corrosion of the suspension steel ties on the maximum deflection of the central main beam of the deck under dead load ($q = 0$) for increasing values of corrosion penetration depth up to collapse.

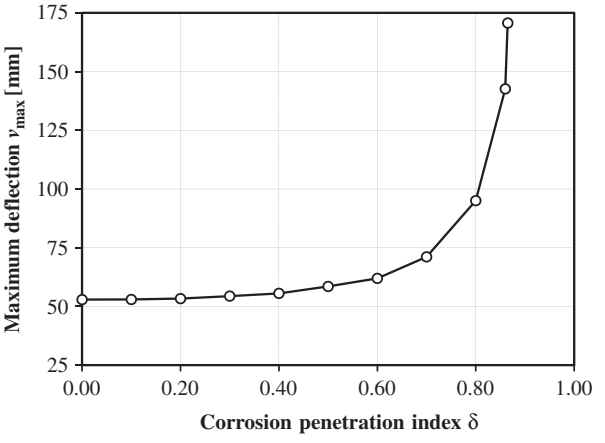

Figure 18. Arch bridge: maximum deflection of the central main beam of the deck under dead load ($q = 0$) versus the corrosion penetration index for the case of bridge with damaged suspension steel ties.

6. Conclusions

A three-dimensional RC beam finite element for nonlinear analysis of concrete structures exposed to corrosion has been presented. The proposed formulation allows to model the damage effects of uniform and pitting corrosion in terms of reduction of cross-sectional area of corroded bars, reduction of ductility of reinforcing steel, deterioration of concrete strength and spalling of concrete cover. The beam finite element has been validated with reference to experimental tests carried out on RC beams subjected to accelerated and natural corrosion. The comparison of experimental and numerical results demonstrated the accuracy of the proposed approach and its capability to reproduce the effects of local corrosion damage on the overall structural response. Moreover, the results of the validation process highlighted the importance of a proper modelling of the delamination and spalling of the concrete cover in compression to accurately predict the initial branch of the load–displacement relationships.

The application to a statically indeterminate RC beam under corrosion showed that design for durability of concrete structures cannot be limited to simplified prescriptions on the quality of the materials and structural detailing, but also needs structural analysis methods capable to take into account the global effects of local damage phenomena on the overall performance of the structure. Finally, the three-dimensional nonlinear structural analysis of a RC arch bridge under different damage scenarios and corrosion penetration levels highlighted the effectiveness and application potentialities of the proposed formulation. In particular, it has been shown how damage can selectively be applied to identify the structural components and members that more significantly affect the system performance when they are exposed to corrosion. This information could provide the basis to establish a hierarchy of protection techniques, as well as to plan proper maintenance actions and repair interventions.

This study focused on the deterministic evaluation of the effects associated with prescribed exposure scenarios and corrosion penetration levels. However, the proposed approach can be extended to account for the uncertainty involved in the problem in probabilistic terms and to include the time factor in a lifetime scale by modelling the diffusive process of aggressive agents leading to corrosion initiation and damage propagation, as described in Biondini et al.(2004a, 2006).

Further developments are needed to include the corrosion of the stirrups and the bond strength deterioration in the damage model and to incorporate the effects of shear behaviour, bond-slip of reinforcement and cyclic loading in the formulation of the deteriorating beam finite element. These factors can be particularly relevant for seismic design and assessment of corroded concrete structures (Akiyama et al., 2011; Biondini et al., 2014).

References

Akiyama, M., Frangopol, D.M., & Matsuzaki, H. (2011). Life-cycle reliability of RC bridge piers under seismic and airborne chloride hazards. *Earthquake Engineering and Structural Dynamics*, *40*, 1671–1687.

Al-Harthy, A.S., Stewart, M.G., & Mullard, J. (2011). Concrete cover cracking caused by steel reinforcement corrosion. *Magazine of Concrete Research*, *63*, 655–667.

Almusallam, A.A. (2001). Effect of degree of corrosion on the properties of reinforcing steel bars. *Construction and Building Materials*, *15*, 361–368.

Alonso, C., Andrade, J., Rodriguez, J., & Diez, J.M. (1998). Factors controlling cracking of concrete affected by reinforcement corrosion. *Materials and Structures*, *31*, 435–441.

ASCE (2013). *Report card for America's infrastructure*. Reston, VA: American Society of Civil Engineers.

Apostolopoulos, C.A., & Papadakis, V.G. (2008). Consequences of steel corrosion on the ductility properties of reinforcement bar. *Construction and Building Materials*, *22*, 2316–2324.

Bhargava, K., Gosh, A.K., Mori, Y., & Ramanujam, S. (2007). Corrosion-induced bond strength degradation in reinforced concrete – Analytical and empirical models. *Nuclear Engineering and Design*, *237*, 1140–1157.

Biondini, F. (2004). A three-dimensional finite beam element for multiscale damage measure and seismic analysis of concrete structures. *13th World Conference on Earthquake Engineering (13 WCEE)*, Vancouver, BC, Canada, 1–6 August, Paper no. 2963.

Biondini, F. (2011). Cellular automata simulation of damage processes in concrete structures. In Y. Tsompanakis & B.H. V. Topping (Eds.), *Soft computing methods for civil and structural engineering*, Chapter 10 (pp. 229–264). Stirlingshire: Saxe-Coburg.

Biondini, F., Bontempi, F., Frangopol, D.M., & Malerba, P.G. (2004a). Cellular automata approach to durability analysis of concrete structures in aggressive environments. *ASCE Journal of Structural Engineering*, *130*, 1724–1737.

Biondini, F., Bontempi, F., Frangopol, D.M., & Malerba, P.G. (2004b). Reliability of material and geometrically nonlinear reinforced and prestressed concrete structures. *Computers & Structures*, *82*, 1021–1031.

Biondini, F., Bontempi, F., Frangopol, D.M., & Malerba, P.G. (2006). Probabilistic service life assessment and maintenance planning of concrete structures. *ASCE Journal of Structural Engineering*, *132*, 810–825.

Biondini, F., Camnasio, E., & Palermo, A. (2014). Lifetime seismic performance of concrete bridges exposed to corrosion. *Structure and Infrastructure Engineering*, *10*, 880–900.

Biondini, F., & Frangopol, D.M. (2008). Probabilistic limit analysis and lifetime prediction of concrete structures. *Structure and Infrastructure Engineering*, *4*, 399–412.

Biondini, F., & Vergani, M. (2012). Damage modeling and nonlinear analysis of concrete bridges under corrosion. *Sixth International Conference on Bridge Maintenance, Safety and Management* (IABMAS 2012), Stresa, Italy, 8–12 July. In F. Biondini & D.M. Frangopol (Eds.), *Bridge Maintenance, Safety, Management, Resilience and Sustainability*. London: CRC Press/Balkema, Taylor & Francis Group.

Bontempi, F., Malerba, P.G., & Romano, L. (1995). Formulazione diretta secante dell'analisi non lineare di telai in C.A./C.A.P. [Secant formulation of nonlinear analysis of RC/PC frames]. In *Studi e Ricerche*, Graduate School for Concrete Structures 'F.lli Pesenti', Politecnico di Milano, Italy, 16, (in Italian) (pp. 351–386).

Castel, A., François, R., & Arliguie, G. (2000). Mechanical behaviour of corroded reinforced concrete beams – Part 1: Experimental study of corroded beams. *Materials and Structures*, *33*, 539–544.

CEB (1992). *Durable concrete structures – Design guide*. Comité Euro-international du Béton, Bulletin d'information no. 183. London: Thomas Telford.

Coronelli, D., & Gambarova, P. (2004). Structural assessment of corroded reinforced concrete beams: Modeling guidelines. *ASCE Journal of Structural Engineering*, *130*, 1214–1224.

Du, Y.G., Clark, L.A., & Chan, A.H.C. (2005). Residual capacity of corroded reinforcing bars. *Magazine of Concrete Research*, *57*, 135–147.

El Maaddawy, T.A., & Soudki, K. (2007). A model for prediction of time from corrosion initiation to corrosion cracking. *Cement and Concrete Composites*, *29*, 168–175.

Ellingwood, B.R. (2005). Risk-informed condition assessment of civil infrastructure: State of practice and research issues. *Structure and Infrastructure Engineering*, *1*, 7–18.

fib (2006). *Model code for service life design*. Bulletin no. 34. Lausanne: fédération internationale du béton/The International Federation for Structural Concrete.

Frangopol, D.M. (2011). Life-cycle performance, management, and optimization of structural systems under uncertainty: Accomplishments and challenges. *Structure and Infrastructure Engineering*, *7*, 389–413.

Frangopol, D.M., & Ellingwood, B.R. (2010). Life-cycle performance, safety, reliability and risk of structural systems, Editorial. *Structure Magazine*, Joint Publication of NCSEA. CASE, SEI. Reedsburg, WI: C_3Ink.

Gonzalez, J.A., Andrade, C., Alonso, C., & Feliu, S. (1995). Comparison of rates of general corrosion and maximum pitting penetration on concrete embedded steel reinforcement. *Cement and Concrete Research*, *25*, 257–264.

Li, C.Q., Zheng, J.J., Lawanwisut, W., & Melchers, R.E. (2007). Concrete delamination caused by steel reinforcement corrosion. *ASCE Journal of Materials in Civil Engineering*, *19*, 591–600.

Lundgren, K. (2007). Effect of corrosion on the bond between steel and concrete: An overview. *Magazine of Concrete Research*, *59*, 447–461.

Malerba, P.G. (Ed.). (1998). *Analisi limite e non lineare di strutture in calcestruzzo armato* [Limit and nonlinear analysis of reinforced concrete structures]. Udine (in Italian): International Centre for Mechanical Sciences (CISM).

NCHRP (2006). *Manual on service life of corrosion-damaged reinforced concrete bridge superstructure elements*. National Cooperative Highway Research Program, Report 558. Washington, DC: Transportation Research Board.

Pantazopoulou, S.J., & Papoulia, K.D. (2001). Modeling cover-cracking due to reinforcement corrosion in RC structures. *ASCE Journal of Engineering Mechanics*, *127*, 342–351.

Rodriguez, J., Ortega, L.M., & Casal, J. (1997). Load carrying capacity of concrete structures with corroded reinforcement. *Construction and Building Materials*, *11*, 239–248.

Rodriguez, J., Ortega, L.M., Casal, J., & Diez, J.M. (1996). Corrosion of reinforcement and service life of concrete structures. In C. Sjostrom (Ed.), *Durability of building materials and components* (Vol. 1, pp. 117–126). London: E & FN Spon.

Sànchez, P.J., Huespe, A.E., Oliver, J., & Toro, S. (2010). Mesoscopic model to simulate the mechanical behavior of reinforced concrete members affected by corrosion. *International Journal of Solids and Structures*, *47*, 559–570.

Stewart, M.G. (2009). Mechanical behaviour of pitting corrosion of flexural and shear reinforcement and its effect on structural reliability of corroding RC beams. *Structural Safety*, *31*, 19–30.

Torres-Acosta, A.A., & Martinez-Madrid, M. (2003). Residual life of corroding reinforced concrete structures in marine environment. *ASCE Journal of Materials in Civil Engineering*, *15*, 344–353.

Val, D.V. (2007). Deterioration of strength of RC beams due to corrosion and its influence on beam reliability. *ASCE Journal of Structural Engineering*, *133*, 1297–1306.

Val, D.V., & Melchers, R.E. (1997). Reliability of deteriorating RC slab bridges. *ASCE Journal of Structural Engineering*, *123*, 1638–1644.

Vergani, M. (2010). *Modellazione del degrado di strutture in calcestruzzo armato soggette a corrosione* [Damage modeling of reinforced concrete structures subjected to corrosion] (Graduate thesis), Milan (in Italian): Politecnico di Milano.

Vidal, T., Castel, A., & Francois, R. (2004). Analyzing crack width to predict corrosion in reinforced concrete. *Cement and Concrete Research*, *34*, 165–174.

Vidal, T., Castel, A., & François, R. (2007). Corrosion process and structural performance of a 17 years old reinforced concrete beam stored in chloride environment. *Cement and Concrete Research*, *37*, 1551–1561.

Vu, K., Stewart, M.G., & Mullard, J. (2005). Corrosion-induced cracking: experimental data and predictive models. *ACI Structural Journal*, *102*, 719–726.

Zhang, R., Castel, A., & François, R. (2009). Concrete cover cracking with reinforcement corrosion of RC beams during chloride-induced corrosion process. *Cement and Concrete Research*, *39*, 1077–1086.